Single Crystal XRD, Bioevaluation and DFT Analysis of 4-Phenylsulfanylbutyric Acid (4PSBA) and Its Cocrystal with 2-Amino-5-nitropyridine (2A5NP)

V. Velmurugan[1], P. Palanisamy[2], R. Subramanian[3], N. Bhuvanesh[4], S. Gomathi[5], P. Thomas Muthiah[5], B. Ravindran Durai Nayagam[6] and S. Kumaresan[7*]

[1]*Department of Chemistry, Manonmaniam Sundaranar University, Tirunelveli-627 012, Tamilnadu, India.*
[2]*Department of Chemistry, Pioneer Kumaraswamy College, Nagercoil-629 003, Tamilnadu, India.*
[3]*Centre for Scientific and Applied Research, SBES, PSN College of Engineering and Technology, Melathediyoor, Tirunelveli- 627 152, Tamilnadu, India.*
[4]*Department of Chemistry, Texas A&M University, College Station, Texas-77842, USA.*
[5]*School of Chemistry, Bharathidasan University, Tiruchirappalli-620 024, Tamilnadu, India.*
[6]*Department of Chemistry, Pope's College, Sawyerpuram-628 251, Tamilnadu, India.*
[7]*Department of Biotechnology, Manonmaniam Sundaranar University, Tirunelveli-627 012, Tamilnadu, India.*

Authors' contributions

This work was carried out in collaboration between all authors. Author SK designed the study and wrote the protocol. Other authors performed the spectral analysis, XRD, DFT etc. All authors read and approved the final manuscript.

Original Research Article

ABSTRACT

The crystal structures of 4-phenylsulfanylbutyric acid (4PSBA) and its cocrystal with 2-amino-5-nitropyridine (2A5NP) have been studied. Both 4PSBA and its co-crystal, 4PSBA:2A5NP belong to the triclinic crystallographic system with the same space group P-1. Theoretical energy calculations

_____

Corresponding author: E-mail: skumarmsu@yahoo.com;

indicated the high energy of the formers 4PSBA and 2A5NP than the cocrystal (4PSBA:2A5NP). The cocrystal has the lowest energy gap (ΔE, 2.9709 eV), lowest hardness (1.4854 eV), highest softness (0.6732 eV), and the highest electrophilicity (5.7412 eV). The cocrystal shows better antimicrobial- and DNA cleaving activity than the acid (4PSBA).

1. INTRODUCTION

Molecular cocrystals have gained importance due to their ability towards physicochemical properties [1,2]. They have been recognized as valuable materials as pharmaceutical cocrystals [3-5]. Improvement of physical properties of cocrystals like solubility, dissolution rate, melting point, color, *etc.* requires proper designing of co-formers [6-8]. Uses of cocrystals include pharmaceutical materials [9], electronic-, and optical materials *etc.* [10,11].

Aminopyridines are an important class of bioactive compounds [12]. The various hydrogen-bonding patterns involving aminopyrimidine–carboxylate interactions have been reported [13]. Recurring of the hydrogen-bonded motifs lead to supramolecular architectures playing a significant role in crystal engineering [14]. Koshima et al. [15,16] reported the syntheses and NLO properties of the cocrystals of 2-amino-5-nitropyridine and benzenesulfonic acids. Fur et al. [17] have reported the noncentrosymmetric structures based on 2-amino-5-nitropyridine and chloroacetic acid assemblies. de Groh and Eric David have demonstrated the ability of 4-phenylsulfanylbutyric acid (4PSBA) to be a novel histone deacetylase inhibitor that stimulates renal progenitor cell proliferation [18]. The present work is focused on the single crystal X-ray diffraction (XRD), and Density Functional Theory (DFT) studies, and biological activity of 4-phenylsulfanylbutyric acid (4PSBA) and its cocrystal with 2-amino-5-nitropyridine (2A5NP).

2. EXPERIMENTAL

2.1 General

The Fourier Transform-Infrared (FT-IR) spectra were recorded in pellet form with spectral grade KBr on a JASCO FT-IR 410 spectrometer in the range 4000–400 cm^{-1}. The single crystal XRD structures of 4-phenylsulfanylbutyric acid (4PSBA) and the cocrystal 4PSBA:2A5NP were determined using a BRUKER APEX 2 X-ray (three-circle) diffractometer.

Intensity data sets were collected at room temperature on a BRUKER SMART APEXII CCD [19] area-detector diffractometer equipped with graphite monochromated Mo Kα radiation (λ = 0.71073 Å). The data were reduced using the program SAINT and empirical absorption corrections were carried out using the SADABS [19]. The structures were solved by direct methods using SHELXS-97 and subsequent Fourier analyses, refined anisotropically by full-matrix least-squares method using SHELXL-97 [20] within the WINGX suite of software, based on F^2 with all reflections. All carbon-hydrogen's were positioned geometrically and refined by a riding model with Uiso1.2 times that of attached atoms. All non-H atoms were refined anisotropically. The molecular structures were drawn using the ORTEP-III [21] and POV-ray [22] programs.

2.2 Computational Methodology

All calculations were performed using Gaussian 09 software [23]. Gas phase geometry was fully optimized at Density Functional Theory (DFT/B3LYP-6-31G(d)) method. The electronic properties were calculated from the Koopmans' theorem and the molecular properties like geometry, total energy, molecular electrostatic potential, E_{HOMO}, E_{LUMO}, dipole moment, electron affinity, ionization potential, chemical potential, electronegativity, absolute hardness, softness, and nucleophilicity were carriedous as reported [24].

2.3 DNA Cleavage Experiment

2.3.1 Preparation of culture media

DNA cleavage experiments were done according to the literature [25]. Nutrient broth was used for the growth of the organism. The 50 mL media was prepared, and autoclaved for 15 min at 121°C and 15 lb pressure. The autoclaved media

were inoculated with the seed culture and incubated at 37℃ for 24 h.

2.3.2 Isolation of DNA

The fresh bacterial culture (1.5 mL) was centrifuged to obtain the pellet which was then dissolved in 0.5 mL of lysine buffer (100 mM Tris pH 8.0, 50 mM EDTA, 10% SDS). To this 0.5 mL of saturated phenol was added and incubated at 55℃ for 10 min and then centrifuged at 10,000 rpm for 10 min. To the supernatant, equal volumes of chloroform:isoamyl alcohol (24:1) and 1/20th volume of 3M sodium acetate (pH 4.8) were added and centrifuged at 10,000 rpm for 10 min. To the supernatant, 3 volumes of chilled absolute alcohol were added. The precipitated DNA was separated by centrifugation and the pellet was dried and dissolved in TAE buffer (10 mM Tris, pH 8.0, 1 mM EDTA) and stored cold.

2.3.3 Agarose gel electrophoresis

Cleavage products were analyzed by agarose gel electrophoresis method [26]. Test samples (1 mg/mL) were prepared in dimethylformamide (DMF). The samples (50 mg) were added to CT DNA and incubated for 2 h at 37℃ and then 20 mL of the DNA sample (mixed with bromophenol blue dye, 1:1 ratio) was loaded carefully into the electrophoresis chamber wells along with standard DNA marker containing TAE (Tris-acetate-EDTA) buffer (pH 8.0) and finally loaded on agarose gel and passed a constant 50 V electricity for around 30 min. The gel was removed and stained with 10 mg/mL ethidium bromide for 10-15 min. The bands were observed under UV transilluminator. Then the results were compared with standard DNA marker.

2.4 DPPH Radical Scavenging Assay

Scavenging effect of 2,2-diphenyl-1-picrylhydrazyl (DPPH) radical was measured according to the procedure described by Blois with a slight modification [26]. Different concentrations (5 μg, 50 μg, and 100 μg) of samples in dimethyl sulfoxide (DMSO), were taken in a series of test tubes. The volume was adjusted to 500 μl by adding methanol. Five milliliters of a 0.1 mM methanolic solution of DPPH (Sigma–Aldrich, Bangalore) was added to these tubes and shaken vigorously. A control without the test compound, but with an equivalent amount of methanol was maintained. The tubes were allowed to stand at room temperature for 20 min. The absorbance of the samples was measured at 517 nm. Ascorbic acid (AA) was used as the reference.

Free radical scavenging activity was calculated using the following formula:

$$\% \text{ Radical scavanching activity} = \frac{(\text{control OD} - \text{sample OD})}{\text{control OD}} \times 100$$

2.5 Investigation of the Antimicrobial Activity

The acid (4PSBA) and the cocrystal (4PSBA:2A5NP) were evaluated for their *in vitro* antibacterial and antifungal activity using agar cup diffusion method. Amikacin was used as a reference. Selected compounds were evaluated for antimicrobial activity by disc diffusion method using Gram-positive bacteria (*Streptococcus pneumoniae, Staphylococcus aureus),* Gram-negative bacteria *(Escherichia coli, Pseudomonas aeruginosa, Proteus vulgaries, and Klebsiella pneumoniae)*, and fungi *(Candida albicans, Aspergillus flavus, Aspergillus niger,* and *Aspergillus fumigatus).*

2.5.1 Preparation of the culture media

All strains were cultured on sterile nutrient agar medium supplied by Sigma- Aldrich, and prepared according to the instructions of the manufactures. The media were molten on a steam bath-inoculated with a few drops of the culture of the specific microorganism, and poured into sterile Petri dishes to form a layer of about 3– 4 mm thickness. The layer was allowed to cool and harden; the underside of each plate was marked into approximately equal six sectors. With the help of a Wassermann tube, a single cup of about 10 mm diameter was cut in the centre of each sector to produce a total of six cups per dish. Five of these cups were allotted for the testing of the desired compounds, while the last one was left as a control guide for the solvent.

2.5.2 Preparation of the solutions of the test compounds

All compounds were first dissolved in $CHCl_3$ in a stock concentration of 1 mg/mL and kept at -20℃ until use. The bacteria cultures were incubated for 24 h at 37℃, and the fungal cultures were incubated for 48 h at 37℃. The inhibition zone diameter was measured in mm. 2-

Amino-5-nitropyridine (2A5NP) was purchased from commercial source (Merck, India). 4-Phenylsulfanylbutyric acid (4PSBA) was synthesized by literature method [27] and single crystals of 4PSBA were obtained from slow evaporation of the saturated solution in hot methanol.

2.6 Synthesis of the Cocrystal 4PSBA:2A5NP

4-Phenylsulfanylbutyric acid (4PSBA) and 2-amino-5-nitropyridine (2A5NP) and of were dissolved separately in 1:1 v/v aqueous methanol. One solution is gradually added into the other with stirring and allowed to stand at room temperature. Slow evaporation of the mixture under ambient conditions yielded colorless crystals of the cocrystal (4PSBA:2A5NP) in 5 days (Yield:

4PSBA:2A5NP, 81%, Anal. Calcd. for $C_{15}H_{17}N_3O_4S$: C, 53.72; H, 5.11; N, 12.53; S, 9.56%. Found: C, 53.65; H, 5.08; N, 12.22 and S, 9.48%.

3. RESULTS AND DISCUSSION

3.1 Crystal Structure

The crystal data, data collection, and refinement details are presented in Table 1. The geometrical parameters of 4-phenylsulfanylbutyric acid (4PSBA) and the cocrystal 4PSBA:2A5NP are listed in Table 2. Some of the weak intermolecular and intramolecular interactions are listed in Table 3. The complete sets of structural parameters are deposited in CCDC of the 4PSBA is 1033657 and cocrystal (4PSBA:2A5NP) is 989252 as a supplementary.

Table 1. Crystal data and structure refinement parameters for 4PSBA and 4PSBA:2A5NP

Identification code	4PSBA	4PSBA:2A5NP
Empirical formula	$C_{10}H_{12}O_2S$	$C_{15}H_{17}N_3O_4S$
Formula weight	196.26	335.38
Temperature	150(2) K	110.15 K
Wavelength	0.71073 Å	0.71073 Å
Crystal system	Triclinic	Triclinic
Space group	P-1	P -1
Unit cell dimensions	a = 6.715(2) Å	a = 6.420(3) Å
	α= 99.371(4)°.	α = 101.874(4)°
	b = 7.699(3) Å	b = 11.024(5) Å
	β= 92.351(4)°	β = 103.294(4)°
	c = 9.582(3) Å	c = 11.775(5) Å
	γ= 94.882(4)°.	γ = 91.032(5)°.
Volume	486.3(3) Å^3	791.8(6) Å^3
Z	2	2
Density (calculated)	1.340 Mg/m^3	1.407 Mg/m^3
Absorption coefficient	0.296 mm^{-1}	0.228 mm^{-1}
F(000)	208	352
Crystal size	0.25 x 0.20 x 0.10 mm^3	0.53 x 0.529 x 0.16 mm^3
Theta range for data collection	2.16 to 27.50°.	1.820 to 27.508°.
Index ranges	-8<=h<=8, -9<=k<=9, -12<=l<=12	-8<=h<=8, -14<=k<=14, -15<=l<=14
Reflections collected	5623	8943
Independent reflections	2195 [R(int) = 0.0240]	3552 [R(int) = 0.0215]
Completeness to theta = 25.242°	98.1	99.5 %
Absorption correction	Semi-empirical from equivalents	Semi-empirical from equivalents
Max. and min. transmission	0.9710 and 0.9297	0.7456 and 0.6547
Refinement method	Full-matrix least-squares on F^2	Full-matrix least-squares on F^2
Data / restraints / parameters	2195 / 0 / 119	3552 / 0 / 209
Goodness-of-fit on F^2	1.071	1.035
Final R indices [I>2sigma(I)]	R1 = 0.0321, wR2 = 0.0831	R1 = 0.0313, wR2 = 0.0846
R indices (all data)	R1 = 0.0358, wR2 = 0.0862	R1 = 0.0362, wR2 = 0.0884
Extinction coefficient	0.409 and -0.220 e.Å-3	n/a

Table 2. Selected bond lengths and bond angles of the acid (4PSBA) and the cocrystal (4PSBA:2A5NP) based on SCXRD and different theoretical studies

Bond length	SCXRD	DFT	HF	MP2	PM3	MM
Co-crystal (4PSBA:2A5NP)						
C(1)-S(1)	1.7611	1.8583	1.8388	1.8653	1.7653	1.8276
S(1)-C(7)	1.8042	1.9180	1.8882	1.9107	1.8289	1.8375
N(2)-O(3)	1.2268	1.2707	1.2301	1.2836	1.2226	1.2245
N(2)-O(4)	1.2353	1.2708	1.2295	1.2840	1.2284	1.2389
C(10)-O(1)	1.2200	1.2519	1.2247	1.2646	1.3547	1.2307
C(10)-O(2)	1.3146	1.3403	1.3278	1.3650	1.2188	1.3293
Acid (4PSBA)						
Bond length	**SCXRD**	**DFT**	**HF**	**MP2**	**PM3**	**MM**
C(1)-S(1)	1.7638	1.8582	1.8381	1.8656	1.7657	1.8275
C(1)-C(7)	1.8055	1.9173	1.8909	1.9104	1.8289	1.8374
C(10)-O(1)	1.2159	1.2302	1.2084	1.2441	1.2062	1.2625
C(10)-O(2)	1.3205	1.3824	1.3513	1.3971	1.3818	1.3938
C(7)-C(8)	1.5231	1.5267	1.5224	1.5316	1.5212	1.5282
C(9)-C(10)	1.4986	1.5028	1.4931	1.5062	1.4979	1.5027
Bond angle	**SCXRD**	**DFT**	**HF**	**MP2**	**PM3**	**MM**
Co-crystal (4PSBA:2A5NP)						
C(1)-S(1)-C(7)	104.78	99.46	100.44	98.02	101.99	102.32
C(8)-C(9)-C(10)	113.07	113.70	113.54	113.04	111.40	112.86
O(1)-C(10)-O(2)	123.33	122.98	122.25	123.42	120.78	122.98
C(9)-C(10)-O(2)	113.01	113.48	113.12	112.68	110.64	112.98
C(9)-C(10)-O(1)	123.66	123.53	124.62	123.88	128.56	122.53
C(7)-C(8)-C(9)	111.12	111.38	110.85	110.92	110.60	111.06
S(1)-C(7)-C(8)	107.27	109.34	109.58	109.67	106.01	106.85
O(3)-N(2)-O(4)	123.39	123.61	123.41	123.92	124.62	123.84
C(12)-N(2)-O(3)	118.50	118.34	118.40	118.14	117.48	118.12
C(12)-N(2)-O(4)	118.11	118.04	118.18	117.93	117.88	117.96
Acid (4PSBA)						
C(1)-S(1)-C(7)	104.47	99.50	100.28	97.21	101.73	102.36
C(8)-C(9)-C(10)	114.13	112.99	113.17	112.54	111.32	112.56
O(1)-C(10)-O(2)	123.39	121.88	121.46	122.09	119.44	120.65
C(9)-C(10)-O(2)	113.00	111.24	111.90	111.12	109.09	112.34
C(9)-C(10)-O(1)	123.61	126.86	126.64	126.78	131.45	124.65
C(7)-C(8)-C(9)	110.06	111.32	111.02	111.17	110.55	110.32
S(1)-C(7)-C(8)	108.87	109.29	109.54	109.48	106.07	108.34

Table 3. Molecular properties of the acid (4PSBA) and the cocrystal (4PSBA:2A5NP) calculated using DFT at the B3LYP/6-311G(d,p) basis set in gaseous phase

Properties	Acid (4PSBA)	Co-crystal (4PSBA:2A5NP)
HOMO (eV)	-5.6971	-5.6154
LUMO (eV)	-0.6167	-2.6445
Energy Gap (ΔE)	5.0804	**2.9709**
IP (eV)	5.6971	5.6154
EA (eV)	0.6167	2.6445
Electronegativity (eV)	3.1569	4.1300
Electrochemical potential (eV)	-3.1569	-4.1300
Hardness (eV)	2.5402	**1.4855**
Softness (eV)	0.3937	**0.6732**
Nucliophilicity (eV)	1.9617	5.7412
Total energy (Kcal/mol)	-936.95	-1445.08
Dipole moment (Debye)	3.6269	3.5261

3.1.1 Crystal structure of 4-phenylsulfanylbutyric acid (4PSBA)

The acid (4PSBA) crystallized in P-1 space group and each asymmetric unit consists of one molecule of the acid. The selected torsion angles of C7-C8-C9-C10, S1-C7-C8-C9, and C1-S1-C7-C8 are -177.67(11)°, 178.13(9)°, and -177.15 (9)°, respectively. The dihedral angle between the phenyl ring and the butyl group is found to be

5.55(6)°. The ORTEP view of the acid (4PSBA) is shown in Fig. 1.

4PSBA molecule forms centrosymmetric dimers *via* a pair of O-H...O hydrogen bonds to form $R_2^2(8)$ homosynthon [28,29]. This motif involves O2 and O1[i] atoms of symmetry related 4PSBA molecules (symmetry code : 3-x, 2-y, 1-z). Two such dimers in a plane are linked by weak C-H...O hydrogen bonds and thus form $R_2^2(24)$ ring motif. This motif links C3 and O1[ii] (symmetry code: x, y, 1+z) atoms of symmetry related 4PSBA molecules. The continuous occurrence of these two ring motifs develop two dimensional supramolecular ribbon extending along the *c* axis as shown in Fig. 2.

The supramolecular ribbons in adjacent layers are connected by C-H...π interaction [30,31] with d(C...π) = 3.689(2)Å and d(H...π) = 2.89Å (Fig. 3). These weak interactions occur between methylene C-H group (C8) and aromatic ring Cg[iii] (symmetry code: 2-x, 1-y, 2-z).

3.1.2 Crystal structure of 4PSBA:2A5NP

4PSBA:2A5NP exists as a 1:1 co-crystal with a P-1 space group. The asymmetric unit consists of one molecule of (2-amino-5-nitropyridine (2A5NP) and one molecule of 4-phenylsulfanylbutyric acid (4PSBA). The ORTEP view of the cocrystal is shown in Fig. 4.

The primary interaction between the acid (4PSBA) and the base (2A5NP) generates a robust $R_2^2(8)$ heterosynthon [32,33] *via* N-H...O and O-H...N hydrogen bonds. This motif links ring N1 and amino N3 atoms of 2A5NP molecule with carboxyl O1 and O2 of 4PSBA molecule. Two such heterosynthons are connected centrosymmetrically *via* a pair of N-H...O hydrogen bonds to form $R_4^2(8)$ ring motif which involves amino N3 of NPA and O1[iii] (symmetry code: 2-x, -y, 1-z) atom of 4PSBA. These interactions generate a DADA array of quadruple hydrogen bonded pattern [34,35] having a fused ring sequences of $R_2^2(8)$, $R_4^2(8)$, and $R_2^2(8)$. The adjacent arrays in a layer are linked *via* weak C-H...O hydrogen bonds and generate $R_2^2(20)$ ring motifs. This motif links inversion related phenyl C-H group (C5) and O2[i] of PSB molecule. (symmetry code: 3-x,1-y,2-z). The alternate occurrences of DADA array and $R_2^2(20)$ ring motif develop supramolecular ribbon extending along the *b* axis. The supramolecular ribbons in successive layers are linked by alternative
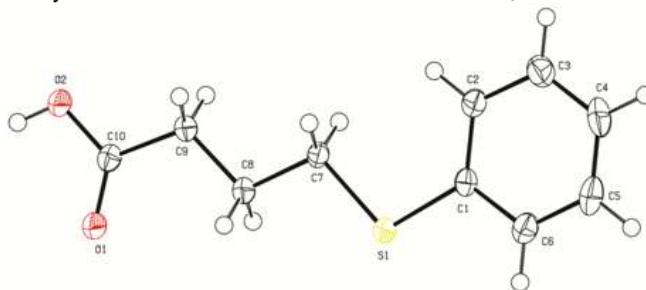

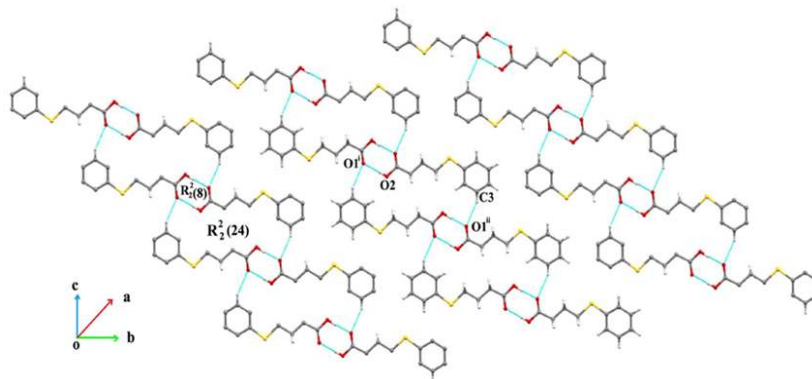**Fig. 1. ORTEP view of 4PSBA with displacement ellipsoids drawn at 50% probability level**

Fig. 2. Supramolecular ribbons through O-H...O and C-H...O hydrogen bonds.
[Symmetry codes: (i) 3-x, 2-y,1-z ; (ii) x, y, 1+z]

occurrences of $R_6^6(26)$ and $R_4^4(34)$ ring motifs. These two motifs are formed *via* weak C-H...O hydrogen bonds and links between phenyl C-H group (C2) of 4PSBA and nitro-O3[ii] of 2A5NP molecule (symmetry code: -2+x, 1+y, z) (Fig. 5).

Further, the crystal structure is stabilized *via* carbonyl-π interactions [36,37] which exists between carbonyl group of 4PSBA and the pyridine ring of 2A5NP (Cg1[iv]) (symmetry code: 3-x,-y,1-z)] of NPA (Fig. 6) with d(C=O...π) = 3.567(2)Å. The carbonyl-π interactions are analogous to anion-π interactions [38,39]. The difference between the pKa values of 2-amino-5-nitropyridine (2.8) and 4-phenylsulfanylbutyric acid (4.49) is ~1.7. Since this difference is not

greater than 3, there is no H-transfer from the carboxylic acid to the amine.
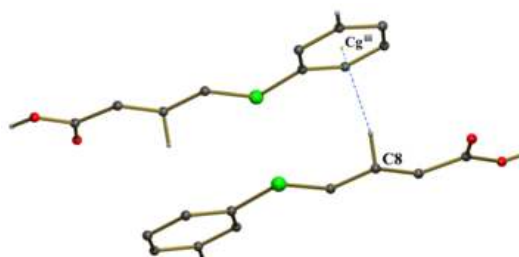
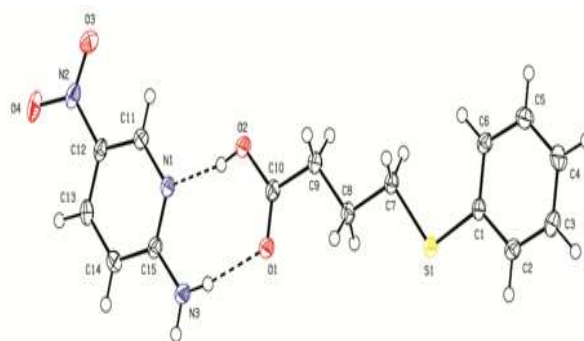**Fig. 3. View of C-H...π interaction [Symmetry code: (iii) 2-x,1-y, 2-z]**

Fig. 4 ORTEP view of 4PSBA:2A5NP with displacement ellipsoids drawn at 50% probability level
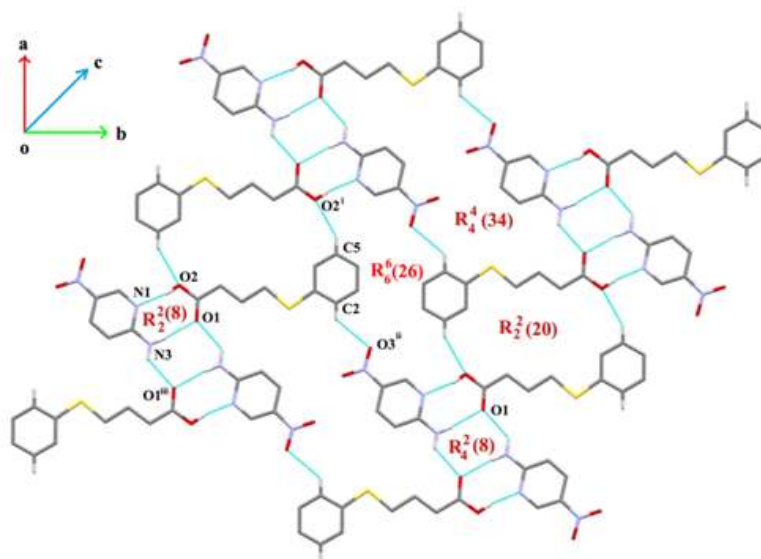

Fig. 5. Supramolecular sheet formed *via* N-H...O. O-H...O and weak C-H...O hydrogen bonds. [Symmetry codes: (i) 3-x,1-y,2-z; (ii) -2+x,1+y, z; (iii) 2-x, -y, 1-z]
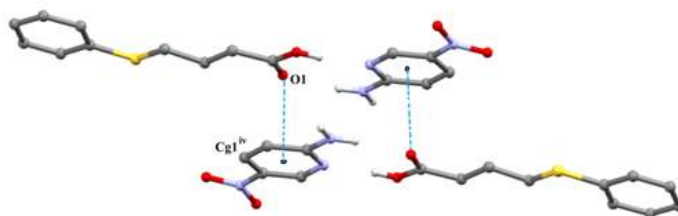
Fig. 6. View of carbonyl-π interaction between C=O...Cg1[iv] [Symmetry codes: (iv) 3-x,-y,1-z]

3.1.3 IR spectrum of the cocrystal (4PSBA: 2A5NP)

The cocrystal 4PSBA: 2A5NP exhibits broad bands in the range 3448-3309 cm^{-1} indicating the intermolecular H-bonded OH group (*vide* Supporting information). Three intense bands were displayed at 1697 cm^{-1}, 1700 cm^{-1} and 1656 cm^{-1}. It is presumed that the stretching frequencies of the amino group of 2A5NP (1639 cm^{-1}), and that of the carboxylic carbonyl (1717 cm^{-1}) of the free acid (4PSBA) merge together and appear as these new bands in the cocrystals. The formation of the new compounds could be confirmed by the changes in the carbonyl frequencies in the crystals. The change in carbonyl frequency in cocrystals is due to the involvement of carboxyl group in hydrogen bond formation.

3.2 Theoretical Studies

Gas phase geometrical parameters of the optimized structure of the acid (4PSBA) and the cocrystal (4PSBA: 2A5NP) at the MM-UFF, MP2, PM3, HF/6-31G(d), and DFT/6-31G(d) levels are listed in Table 2. The DFT method represents good correlation between the calculated geometrical parameters and the single crystal XRD (SCXRD) data. This method also helps in the calculation of the other parameters for the acid (4PSBA) and the cocrystal (4PSBA:2A5NP). Table 2 reveals that the geometrical parameters of theoretical studies are nearly the same as the experimental ones for the acid (4PSBA) and the cocrystal (4PSBA: 2A5NP). The acid (4PSBA) and the cocrystal (4PSBA: 2A5NP) have been studied theoretically in the absence of their SCXRD data using the B3LYP/3-21G(d) level of theory [40]. In total we have investigated the electronic structures of the acid (4PSBA) and the cocrystal (4PSBA: 2A5NP) using the DFT method. Fig. 7 shows the optimized structures of the acid (4PSBA) and the cocrystal (4PSBA:2A5NP). Cocrystal (4PSBA:2A5NP)

(-1445.08) has lower energy than the acid (4PSBA) (-936.95).

3.2.1 Molecular Electrostatic Potential (MEP)

Molecular electrostatic potential (MEP) maps provide the isosurface values with the location of negative and positive electrostatic potentials. The differences between nuclophilicity and electrophilicity may affect the proton donating/accepting ability of a compound [41]. Negative electrostatic potential corresponds to the attraction of the proton by the high electron density in the molecule (and is colored in the shades of red on the EPS surface). Positive electrostatic potential corresponds to the repulsion of the proton by atomic nuclei in regions where low electron density exists and the nuclear charge is incompletely shielded (and is colored in shades of blue) [42]. Fig. 8 shows the MEP of the acid (4PSBA) and the cocrystal (4PSBA:2A5NP) determined using DFT/B3LYP 6-31G(d) method. The different values of the electrostatic potential at the surface are represented by different colors. As can be seen in Fig. 8, the negative (red) region is localized on the carbonyl oxygen (O2) and sulphur. However, positive (blue) region is localized on the nitrogen probably due to the hydrogen atoms and the green represents regions of zero potential. Therefore, Fig. 8 confirms the existence of an intermolecular N-H….O bonding. The pale red and blue regions reveal the presence of weak interactions. Hence, it can be said these color differences give the information about the region from where the compound can have N–H.....π, and C–H.....π intermolecular interactions in the acid (4PSBA) and the cocrystal (4PSBA:2A5NP) in the gaseous phase. These interactions were confirmed in acid (4PSBA) and cocrystal (4PSBA:2A5NP) from both theoretical and SCXRD studies. The optimized structures of the acid (4PSBA) and the cocrystal (4PSBA:2A5NP) also have similar types of MEP and may have the same interactions, excepting that the molecular electrostatic potential value is different.
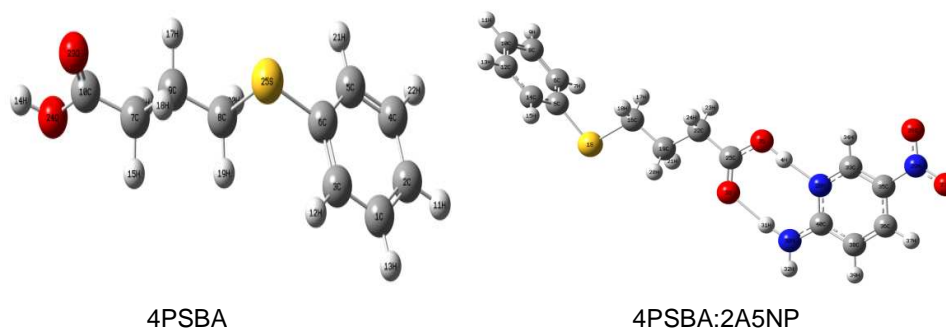
4PSBA   4PSBA:2A5NP

Fig. 7. Optimized structures of acid (4PSBA) and cocrystal (4PSBA:2A5NP)

MEP of the acid (4PSBA)
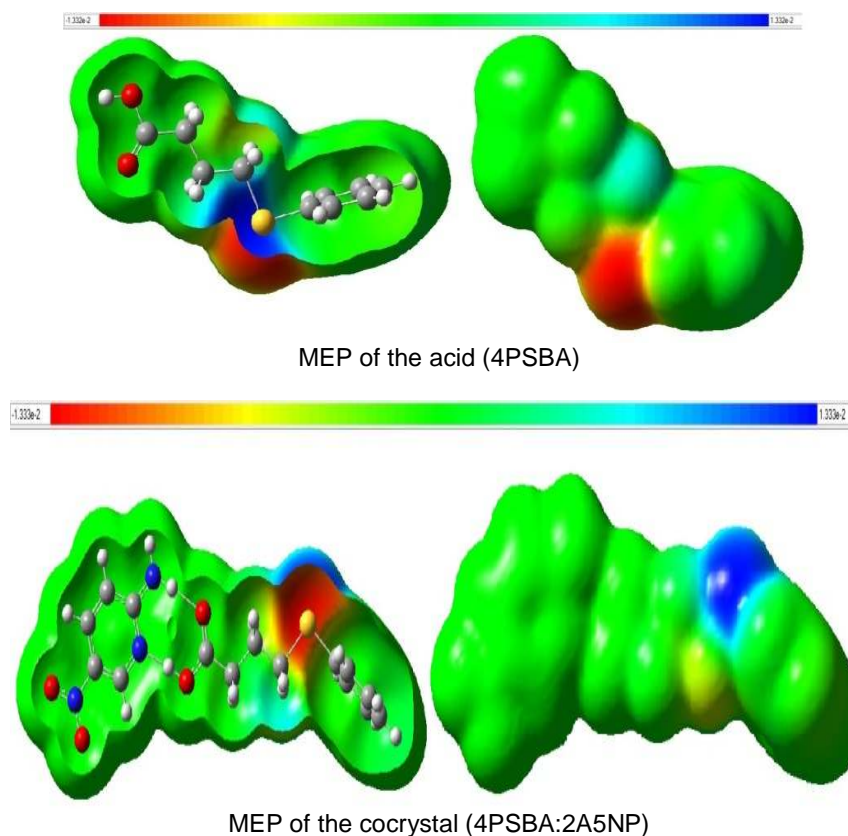

MEP of the cocrystal (4PSBA:2A5NP)

Fig. 8. Molecular electrostatic potential of 4PSBA and 4PSBA:2A5NP

3.2.2 Frontier molecular orbitals

Frontier molecular orbitals (FMO) could provide information regarding the inverse dependence of stabilization energy on orbital energy difference. E_{HOMO} is generally associated with the electron donating ability of a molecule. High values of E_{HOMO} are likely to denote the tendency of the molecule to donate electrons to acceptor molecules of lower energy MO. E_{LUMO}, indicates the ability of the molecule to accept electrons [43]. The binding ability of the molecule increases with increasing HOMO and decreasing LUMO energy values. Thus, the lower the value of E_{LUMO}, the most probable it is that the molecule would accept electrons. Figs. 9 and 10 reveal the HOMO and LUMO of the acid (4PSBA) and the cocrystal (4PSBA:2A5NP). From this, one can understand that cocrystal (4PSBA:2A5NP) has the highest E_{HOMO} value (-5.6154eV) and lowest E_{LUMO} (-2.6445) value.
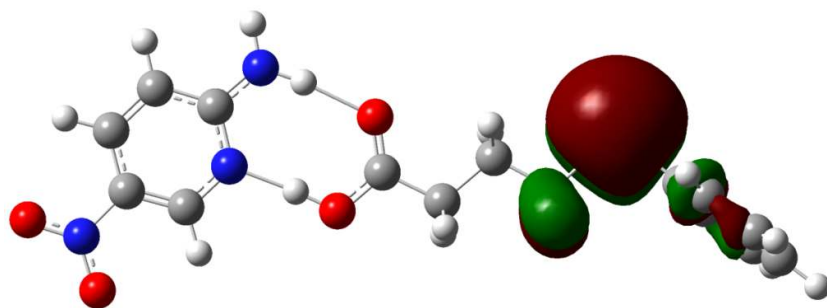
9

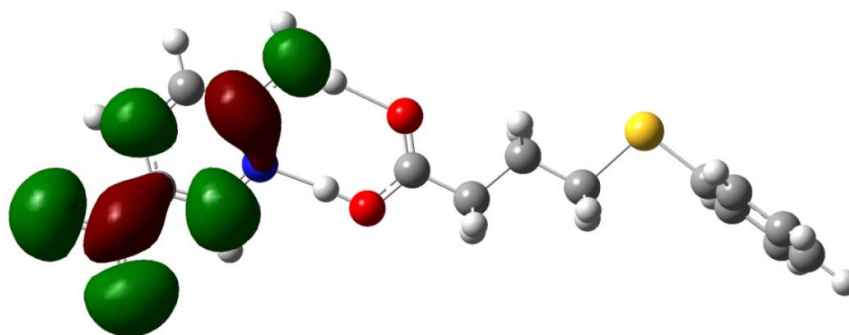**Fig. 9. HOMO of the cocrystal (4PSBA:2A5NP)**

Fig. 10. LUMO of the cocrystal (4PSBA:2A5NP)

The difference between the HOMO and LUMO energy levels (DE) of the molecule is an important parameter determining the reactivity of the molecule. As DE decreases (especially for the cationic species), the reactivity of the molecule increases making the molecule less stable. Table 3 reveals that the HOMO–LUMO energy gap of the cocrystal (4PSBA:2A5NP) is lower than that of acid (4PSBA).

The dipole moment, which is defined as the first derivative of the energy with respect to an applied electric field, is mainly used to study the intermolecular interactions such as van der Waals type dipole–dipole forces etc. The larger the dipole moment the stronger will be the intermolecular attraction [44]. The acid has higher dipole moment (3.6269 D) which reveals it to be more polar than the cocrystal. Absolute hardness, g, and softness, r, are important properties to measure the molecular stability and reactivity. A hard molecule has a large energy gap and a soft molecule has a small energy gap. Soft molecules are more reactive than hard ones because they could easily offer electrons to an acceptor. For the simplest transfer of electrons, absorption could occur at the part of the molecule where r has the highest magnitude whereas g has the lowest [45]. The

nucleophilicity, x, measures the electrophilic power of a molecule. It has been reported that the lower the value of x, the lower the capacity of the molecule to donate electrons [46]. Table 3 shows that cocrystal (4PSBA:2A5NP) has lower energy gap (DE, 2.9709 eV).

Lower hardness (1.4854 eV), the higher softness (0.6732 eV), and a higher electrophilicity (5.7412 eV). These data agree with the experimental results that the cocrystal (4PSBA:2A5NP) shows better antimicrobial-, and DNA cleaving ability. The acid (4PSBA) has the higher energy gap (5.0804 eV), higher hardness (2.5402 eV), and a lower softness (0.3937 eV).

According to the molecular orbital (MO) theory, HOMO and LUMO are the most important factors affecting the bioactivity. The interaction between these molecules and the receptor of bacteria are correlated to π–π or hydrophobic interaction among these frontier molecular orbitals. If the charged parameters are responsible for antimicrobial activity of these molecules, then the negative charges mainly located on carbonyl O-atom may be said to interact with the positive portion of the receptor. The N–H and C–H, being the most positively charged parts, can interact with the negatively charged region of the

receptor easily. We have finally resolved that the HOMO and LUMO of the cocrystal is mostly having π-antibonding type orbitals and thus, the electronic transitions from the HOMO to LUMO are mainly derived from the contribution of π–π* bands [47]. This is in agreement with the cocrystal (4PSBA:2A5NP) exhibiting higher biological activity.

3.3 TGA/DTA Measurement for the Cocrystal (4PSBA:2A5NP)

TGA studies indicated that **4PSBA:2A5NP** underwent a complete decomposition starting from170℃ to 270℃ leading to a weight loss of 96.1% (Fig. 11, *vide* Supporting information). Thus the co-crystal is thermally stable up to 170℃. However, the DTA curve indicated an endothermal reaction in the temperature range 170℃-270℃.

3.4 DNA Cleavage Studies

The DNA cleavage studies of the acid (4PSBA) and the cocrystal (4PSBA:2A5NP) have been carried out against CT DNA by agarose gel electrophoresis method (Fig. 12). The acid (4PSBA) sample has partially cleaved DNA at all concentrations, but the cocrystal (4PSBA:2A5NP) has completely cleaved DNA at 125 and 250 µg concentrations, and a partial cleavage at 50 µg concentration. The acid and cocrystal have clearly showed the absence of marker band thus providing a proof for the complete cleavage of CT DNA. It can be concluded that 4PSBA as well as 4PSBA:2A5NP inhibit the growth of the pathogenic organisms by cleaving the genome.

3.5 Free Radical Scavenging Activity

The free radical-scavenging activity for the acid (4PSBA) and cocrystal (4PSBA:2A5NP) was evaluated using DPPH model system and the results are presented in Table 4. From the results it is clear that the free radical-scavenging activities of the cocrystal are slightly greater than that of the acid.

3.6 Antimicrobial Activity

The antimicrobial activity was assayed using the cup-plate agar diffusion method [48] by measuring the zone of inhibition in mm. The acid (4PSBA) and cocrystal (4PSBA:2A5NP) were screened *in vitro* for their antimicrobial activity against varieties of Gram-positive bacteria (*Streptococcus pneumoniae, Staphylococcus aureus*), Gram-negative bacteria (*Escherichia coli, Pseudomonas aeruginosa, Proteus vulgaris, and Klebsiella pneumoniae*) and fungi (*Candida albicans, Aspergillus flavus, Aspergillus niger, and Aspergillus fumigatus*) at 40 µg/mL concentration. Amikacin and Nystatin were used as standards for comparison purpose of antibacterial and antifungal activity. The results are given in Tables 5 and 6.

Table 4. DPPH radical-scavenging activity of acid (4PSBA) and cocrystal (4PSBA:2A5NP)

Concentration	DPPH radical scavenging (%)		
	4PSBA	4PSBA:2A5NP	Ascorbic acid standard
10 µg/mL	0.36	0.86	21.62
50 µg/mL	3.14	5.12	75.34
100 µg/mL	6.94	11.02	96.15
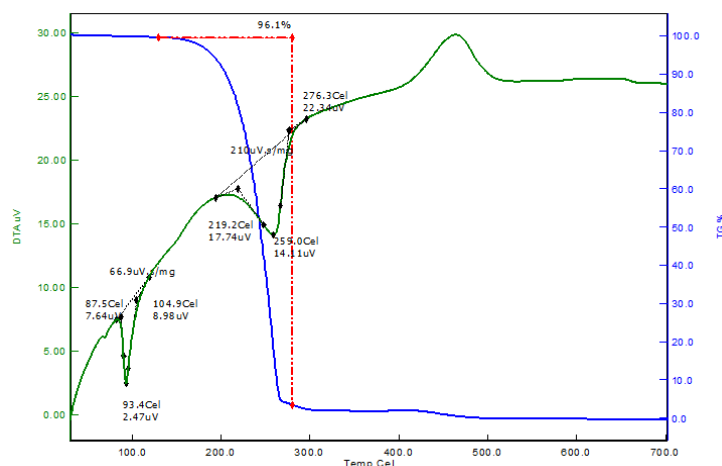
Fig. 11. TGA analysis of co-crystal

Table 5. Antibacterial activity

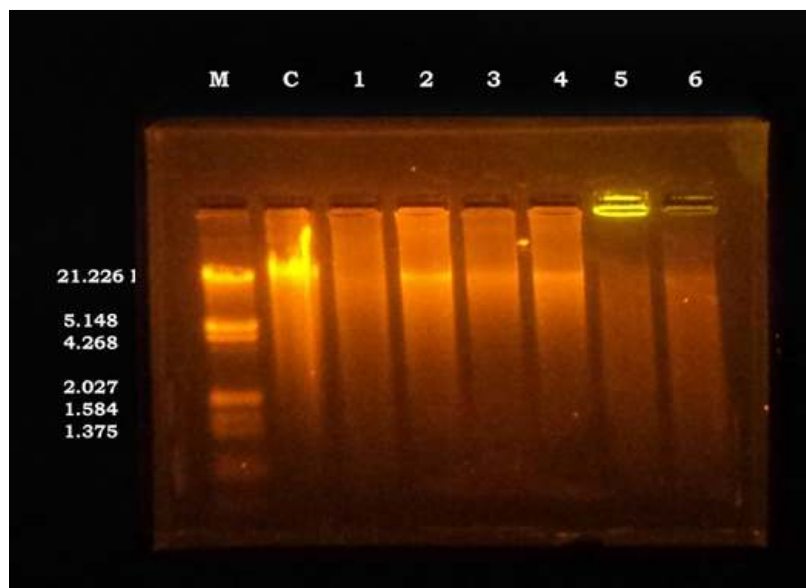| Compounds	Zone of inhibition (mm)					
	Gram negative bacteria				Gram positive bacteria	
	Klebsiella pneumoniae	*Pseudomonas aeruginosa*	*Proteus vulgaris*	*Escherichia coli*	*Streptococcus pneumoniae*	*Staphylococcus aureus*
Acid (4PSBA)	16	12	10	19	14	16
Cocrystal (4PSBA:2A5NP)	32	16	11	31	19	24
Amikacin standard	29	25	15	30	18	22

Fig. 12. Gel electrophoresis picture of 4PSBA and 4PSBA:2A5NP showing the effect on CT-DNA
Lane M: DNA marker. Lane C: untreated DNA; Lane 1. 4PSBA 50 μg, Lane 2. 4PSBA 125 μg, Lane 3. 4PSBA 250 μg, Lane 4. 4PSBA:2A5NP 50 μg, Lane 5. 4PSBA:2A5NP 125 μg, Lane 6. 4PSBA:2A5NP 250 μg concentration

Table 6. Antifungal activity

Compounds	Zone of inhibition(mm)			
	Fungi			
	Candida albicans	*Aspergillus flavus*	*Aspergillus fumigatus*	*Aspergillus niger*
Acid (4PSBA)	29	10	15	13
Cocrystal (4PSBA:2A5NP)	33	12	19	15
Nystatin standard	32	25	18	27

Results indicate that the acid (4PSBA) and the cocrystal (4PSBA:2A5NP) exhibited reasonable antibacterial and antifungal activity. Cocrystal has better bioactivity against *Klebsiella pneumoniae, Streptococcus pneumoniae, Escherichia coli, Candida albicans, and Aspergillus fumigatus* compared to the standards, Amikacin and Nystatin. Simillarly the cocrystal has moderate activity against *Pseudomonas aeruginosa, Proteus vulgaris, Aspergillus flavus,* and *Aspergillus niger.* Results show that the antimicrobial activities of the cocrystals are better than that of the acid.

4. CONCLUSIONS

Single crystal XRD, and DFT studies were made on 4-phenylsulfanylbutyric acid (4PSBA) and its cocrystal (4PSBA:2A5NP). The cocrystal forms two-component assemblies based on the well-established 2-amino-5-nitropyridine–carboxylic acid synthon. The crystal structure is stabilized *via* carbonyl-π interactions that exist between the carbonyl group of 4PSBA and pyridine ring of 2A5NP. The carbonyl-π interactions are analogous to anion-π interactions. The cocrystal possesses less energy gap, less hardness, more softness and more nucleophilicity; this agrees with the experimental results that the cocrystal shows better DNA cleaving-, free radical-scavenging-, and antimicrobial activity.

COMPETING INTERESTS

Authors have declared that no competing interests exist.

REFERENCES

1. Desiraju GR. Crystal and co-crystal. Cryst. Eng. Commun. 2003;5:466.
2. Dunitz JD. Crystal and co-crystal: A second opinion. Cryst. Eng. Commun. 2003;5:506.
3. Panunto TW, Lipkowska ZU, Johnson R, Etter MC. Hydrogen-bond formation in nitroanilines: The first step in designing acentric materials. J. Am. Chem. Soc. 1987;109:7786.
4. Etter MC, Lipkowska ZU, Mohammad Zia-Ebrahimi S, Panunto TW. Hydrogen bond-directed cocrystallization and molecular recognition properties of diarylureas. J. Am. Chem. Soc. 1990;112:8415.
5. Etter MC, Reutzel SM, Choo CG. Self-organization of adenine and thymine in the solid state. J. Am. Chem. Soc. 1993;115: 4411.
6. Zaworotko M. N′-[4-(Dimethylamino) benzylidene]-3-hydroxybenzohydrazide. Acta Cryst. 2008;A64:c11.
7. Sun CC, Hou H. Improving mechanical properties of caffeine and methyl gallate crystals by cocrystallization. Cryst. Growth Des. 2008;8:1575.
8. Horendo NR, Nehm SJ, Jayasankar A. Cocrystals: Design, properties and formation mechanisms. Encyclopedia of Pharmaceutical Technology, Third Ed. Taylor & Francis, London. 2007;815.
9. (a) Trask AV, Motherwell WDS, Jones W, Pharmaceutical cocrystallization: Engineering a remedy for caffeine hydration. Cryst. Growth Des. 2005;5:1013; (b) Vishweshwar P, McMahon JA, Bis JA, Zaworotko MJ. Pharmaceutical co-crystals. J. Pharm. Sci. 2006;95:499; (c) McNamara DP, Childs SL, Giordano J, Iarriccio A, Cassidy J, Shet MS, Mannion R, O'Donnell E, Park A. Nicotinamide: Fumaric acid supramolecular cocrystals: Diversity of stoichiometry. Pharm. Res. 2006;23:1888; (d) Jayasankar A, Somwangthanaroj A, Shao ZJ, Hornedo NR. Cocrystal formation during cogrinding and storage is mediated by amorphous phase. Pharm. Res. 2006;23:2381; (e) Nehm SJ, Spong BR, Hornedo NR. Phase solubility diagrams of cocrystals are explained by solubility product and solution complexation. Cryst. Growth Des. 2006;6:592.
10. (a) Sokolov AN, Frišcíc´ T, MacGillivray LR. Enforced face-to-face stacking of

organic semiconductor building blocks within hydrogen-bonded molecular cocrystals. J. Am. Chem. Soc. 2006;128: 2806; (b) Papaefstathiou GS, Zhong Z, Geng L, MacGillivray LR. Coordination-driven self-assembly directs a single-crystal-to-single-crystal transformation that exhibits photocontrolled fluorescence. J. Am. Chem. Soc. 2004;126:9158.

11. (a) Cheney ML, McManus GJ, Perman JA, Wang Z, Zaworotko MJ. The role of cocrystals in solid-state synthesis: Cocrystal-controlled solid-state synthesis of imides. Cryst.Growth Des. 2007;7:616; (b) Friscic T, MacGillivray LR. Engineering cocrystal and polymorph architecture via pseudo seeding. Chem. Commun. 2006; 5748; (c) Gao X, Friščic´ T, MacGillivray LR. Supramolecular construction of molecular ladders in the solid state. Angew. Chem. Int. Ed. 2004;43:232; (d) Kim JH, Lindeman SV, Kochi JK. Charge-transfer forces in the self-assembly of heteromolecular reactive solids: Success-ful design of unique (single-crystal-to-single-crystal) Diels-Alder cycloadditions. J. Am. Chem. Soc. 2001;123:4951.

12. Baltork IM, Moghadam M, Tangestaninejad S, Mirkhani V, Zolfigol MA, Hojati SF. Silica sulfuric acid catalyzed synthesis of benzoxazoles, benzimidazoles and oxazolo [4, 5-b] pyridines under hetero-geneous and solvent-free conditions, J. Iran. Chem. Soc. 2008;5:S65–S70.

13. Stanley N, Muthiah PT, Geib SJ, Luger P, Weber M, Messerschmidt M. Tetrahedron. 2005;61:7201–7210.

14. Stanley N, Muthiah PT, Geib SJ, Luger P, Weber M, Messerschmidt M. The novel hydrogen bonding motifs and supramolecular patterns in 2,4-diaminopyrimidinenitrobenzoate complexes. Tetrahedron. 2005;61:7201–7210.

15. Lynch DE, Jones GD. Geometry of the 2-aminoheterocyclic–carboxylic acid R22 (8) graph set: Implications for crystal engineering. Acta Crystallogr. B. 2004;60: 748–754.

16. Koshima H, Hamada M, Yagi I, Uosaki K, Synthesis, structure and second-harmonic generation of chiral and noncentro-symmetric salt crystals of 2-Amino-5-nitropyridine with achiral benzenesulfonic acids. Crystal Growth & Design. 2001;1(6):467-471.

17. Koshima H, Miyamoto H. Cocrystals of 2-Amino-5-nitropyridine with Benzenesulfonic acids for second order nonlinear optical materials. Mol. Cryst. Liq. Cryst. 2004;414:77–86.

18. Fur YL, Beucher MB, Masse R, Nicoud JF, Levy JP. Crystal engineering of noncentrosymmetric structures based on 2-amino-5-nitropyridine and n-chloroacetic acid assemblies, Chem. Mater. 1996;8:68-75. [18-a] de Groh E David Ph.D Disseration, University of Pittsburgh, USA; 2010.

19. Bruker APEX2, SAINT and SADABS, Bruker AXS Inc., Madison, Wisconsin, USA; 2008.

20. Sheldrick GM. A short history of SHELX. Acta Cryst. 2008;A64:112.

21. Spek AL. Single-crystal structure validation with the program PLATON. Acta Cryst. 2009;D65:148.

22. Farrugia LJ. POV-Ray– 3.5. Glasgow University, Australia; 2003.

23. Frisch MJ, Trucks GW, Schlegel HB, Scuseria GE, Robb MA, Cheeseman JR, Scalmani G, Barone V, Mennucci B, Petersson GA, Nakatsuji H, Caricato M, Li X, Hratchian HP, Izmaylov AF, Bloino J, Zheng G, Sonnenberg JL, Hada M, Ehara M, Toyota K, Fukuda R, Hasegawa J, Ishida M, Nakajima T, Honda Y, Kitao O, Nakai H, Vreven T, Montgomery JA Jr, Peralta JE, Ogliaro F, Bearpark M, Heyd JJ, Brothers E, Kudin KN, Staroverov VN, Kobayashi R, Normand J, Raghavachari K, Rendell A, Burant JC, Iyengar SS, Tomasi J, Cossi M, Rega N, Millam JM, Klene M, Knox JE, Cross JB, Bakken V, Adamo C, Jaramillo J, Gomperts R, Stratmann RE, Yazyev O, Austin AJ, Cammi R, Pomelli C, Ochterski JW, Martin RL, Morokuma K, Zakrzewski VG, Voth GA, Salvador P, Dannenberg JJ, Dapprich S, Daniels AD, Farkas O, Foresman JB, Ortiz JV, Cioslowski J, Fox DJ. Gaussian, Inc., Wallingford, CT; 2009.

24. Suresh Kumar GS, Antony Muthu Prabu A, Jegan Jenniefer S, Bhuvanesh N, Thomas Muthiah P, Kumaresan S. Syntheses of phenoxyalkyl esters of 3, 3'-bis(indolyl)methanes and studies on their molecular properties from single crystal XRD and DFT techniques. J. Mol. Str. 2013;1047:109–120.

25. Brown TA. Molecular biology, Practical Approach. 1990;1:51-52.

26. Kumar S, Kumar D, Manjusha S, Saroha K, Singh N, Vashishta B. Antioxidant and free radical scavenging potential of *Citrullus colocynthis* (L.) Schrad. methanolic fruit extract. Acta. Pharm. 2008;58:215–220.

27. Doria G, Isetta AM, Ferrari M, Trizio D. Syntheses, characterization, antimicrobial, antituberculosis, and antitumor activity of N, 1-Diphenyl-1, 4-dihydrothiochromeno [4,3-c] pyrazole-3-carboxamide. Eur. Pat. Appl. 1988;88:300115.

28. Wang J, Xiang J, Wu A, Meng X. Robust R^2_2 (8) hydrogen bonded dimer for crystal engineering of glycoluril derivatives. Cryst. Eng. Comm. 2013;15:10079–10085

29. Gomathi S, Muthiah PT. 2-Amino-4, 6-dimethoxypyrimidin-1-ium p-toluenesulfonate, Acta Cryst. 2013;E69: 1235.

30. Babu MM. Nucleic Acids Research. 2003;31(13):3345–3348.

31. Kumar RM, Elango M, Parthasarathi R, Vijay D, Subramanian V. The role of C–H...π interaction in the stabilization of benzene and adamantane clusters. J. Chem. Sci. 2012;124(1):193–202.

32. Khan M, Enkelmann V, Brunklaus G. Heterosynthon mediated tailored synthesis of pharmaceutical complexes: A solid-state NMR approach. Crystal Growth & Design. 2009;9(5):2354-2362.

33. Adalder TK, Sankolli R, Dastidar P. Homo- or Heterosynthon? A crystallographic study on a series of new cocrystals derived from pyrazinecarboxamide and various carboxylic acids equipped with additional hydrogen bonding sites. Cryst. Growth Des. 2012;12:2533–2542.

34. Sherrington DC, Taskine KA. Self-assembly in synthetic macromolecular systems via multiple hydrogen bonding interactions. Chem. Soc. Rev. 2001;30:83–93.

35. Thanigaimani K, Muthiah PT. Hydrogen-bonded supramolecular motifs in pyrimethaminium 4-methylbenzoate, pyrimethaminium 3-hydroxypicolinate and pyrimethaminium 2,4-dichlorobenzoate. Acta Cryst. 2010;C66:o104-o108.

36. Gao XL, Lu LP, Zhu ML. The crucial role of C—H··· O and C= O··· π interactions in the building of three-dimensional structures of dicarboxylic acid–biimidazole compounds. Acta Cryst. 2009;C65:o123–o127.

37. Gautrot JE, Hodge P, Cupertino D, Helliwell M. Experimental evidence for carbonyl–π electron cloud interactions. New J. Chem. 2006;30:1801–1807.

38. Babu MM. Nucleic Acids Research. 2003;31(13):3345–3348.

39. Kumar RM, Elango M, Parthasarathi R, Vijay D, Subramanian V. The role of C–H...π interaction in the stabilization of benzene and adamantane clusters. J. Chem. Sci. 2012;124(1):193–202.

40. [40] (a) Chattaraj PK, Lee H, Parr RG, HSAB principle. J. Am. Chem. Soc. 1991;113:1855; (b) Linder M, Brinck T, Stepwise Diels–Alder: More than just an oddity? A computational mechanistic study. J. Org. Chem. 2012;77:6563

41. Yesilkaynak T, Binzet G, Emen FM, Florke U, Kulcu N, Arslan H. Theoretical and experimental studies on N-(6-methylpyridin-2-yl-carbamothioyl) biphenyl-4-carboxamide. Eur. J. Chem. 2010;1(1):1.

42. Mishra S, Chaturvedi D, Kumar N, Tandon P, Siesler HW. An ab initio and DFT study of structure and vibrational spectra of γ form of Oleic acid: Comparison to experimental data. Chem. Phys. Lipids. 2010;163:207.

43. Ahamad I, Prasad R, Quraishi MA. Mater, anticorrosion potential of 2-Mesityl-1H-imidazo[4,5-f][1,10]phenanthroline on mild steel in sulfuric acid solution: Experimental and theoretical study. Chem. Phys; 2010. Available:http://dx.doi.org/10.1016/j.match emphys.2010.08.051

44. Bouklah M, Harek H, Touzani R, Hammouti B, Harek Y, Experimental and quantum chemical characterization of the adsorption of some Schiff base compounds of phthaloyl thiocarbo-hydrazide on the mild steel in acid solutions Arab. J. Chem. Available:http://dx.doi.org/10.1016/j.arabjc. 2010.08.008

45. Obi-Egbedi NO, Obot IB. Inhibitive properties, thermodynamic and quantum chemical studies of alloxazine on mild steel corrosion in H_2SO_4. Corros. Sci. Available:http://dx.doi.org/10.1016/ j.corsci.2010.09.020

46. Masoud MS, Awad MK, Shaker MA. El-Tahawy MMT. The role of structural chemistry in the inhibitive performance of some aminopyrimidines on the corrosion of steel. Corros. Sci. 2010;52:2387–2396.

47. Obot IB, Johnson AS. Ab initio, DFT and TD-DFT electronic absorption spectra

investigations on 3,5-diamino-1,2,4-triazole, Elxir Comp. Chem. 2012;43:6658–6661.

48. (a) Barry AL. In the antimicrobial susceptibility test: Principle and practices; Lea I.; Febiger, Eds.; CBS Publishers and Distributors, Philadelphia, PA, USA; 1976;180; (b) Barry AL. The antimicrobial susceptibility test, principle and practices. Biol. Abstr. 1976;64:25183.

Peer-review history:
The peer review history for this paper can be accessed here:
http://sciencedomain.org/review-history/13899